

# A collimated jet and an infalling-rotating disk in G192.16–3.84 traced by H<sub>2</sub>O maser emission

Hiroshi IMAI<sup>1</sup>, Toshihiro OMODAKA<sup>1</sup>, Tomoya HIROTA<sup>2</sup>, Tomofumi UMEMOTO<sup>3</sup>,  
Kazuo SORAI<sup>4</sup>, and Tetsuro KONDO<sup>5</sup>

<sup>1</sup>*Department of Physics, Faculty of Science, Kagoshima University, Kagoshima 890-0065*

<sup>2</sup>*Mizusawa VERA Observatory Mitaka Office, National Astronomical Observatory, Mitaka, Tokyo 181-8588*

<sup>3</sup>*Nobeyama Radio Observatory, National Astronomical Observatory,  
Minamimaki, Minamisaku, Nagano 384-1305*

<sup>4</sup>*Division of Physics, Graduate School of Science, Hokkaido University, Sapporo 060-0810*

<sup>5</sup>*Kashima Space Research Center, National Institute of Information and Communication Technology,  
Kashima, Ibaraki 314-0012*

(HI) [hiroimai@sci.kagoshima-u.ac.jp](mailto:hiroimai@sci.kagoshima-u.ac.jp)

(Received 2006 May 18; accepted 2006 August 14)

## Abstract

We report H<sub>2</sub>O masers associated with the massive-star forming region G192.16–3.84 observed with the new Japan VLBI network at three epochs spanned for two months, which have revealed the three-dimensional kinematical structure of the whole H<sub>2</sub>O maser region in G192.16–3.84, containing two young stellar objects separated by  $\sim 1200$  AU. The maser spatio-kinematical structure has well persisted since previous observations, in which the masers are expected to be associated with a highly-collimated bipolar jet and an infalling-rotating disk in the northern and southern clusters of H<sub>2</sub>O maser features, respectively. We estimated a jet expansion speed of  $\sim 100$  km s<sup>-1</sup> and re-estimated a dynamical age of the whole jet to be  $5.6 \times 10^4$  yrs. We have investigated the spatial distribution of Doppler velocities during the previous and present observations and relative proper motions of H<sub>2</sub>O maser features

in the southern cluster, and a relative bulk motion between the two maser clusters. They are well explained by a model of an infalling–rotating disk with a radius of  $\sim 1000$  AU and a central stellar mass of  $5\text{--}10 M_{\odot}$ , rather than by a model of a bipolar jet perpendicular to the observed CO outflow. Based on the derived H<sub>2</sub>O maser spatio-kinematical parameters, we discuss the formation mechanism of the massive young stellar objects and the outflow development in G192.16–3.84.

**Key words:** masers — stars:formation — stars:mass accretion — stars:individual (G192.16–3.84) — ISM:jets and outflows

## 1. Introduction

Formation mechanism of massive stars is one of the most important issues in astrophysics for elucidating their whole evolution as well as their effects on dynamical and chemical composition evolution of galaxies and the universe. It is difficult, however, to observationally find the true mechanism because all of massive young stellar objects (MYSOs) are associated with star clusters that are deeply embedded in molecular clouds located at large distances from the Sun ( $d \gtrsim 500$  pc). Therefore, in whichever scenario of massive star formation, observations with very high angular resolution (better than 10 milliarcseconds, mas) is essential to resolve a massive-star forming region into individual MYSOs. Because a massive star also evolves extremely rapidly, it is difficult to find MYSOs at the earliest stage of the star formation process. An MYSO with  $M \gtrsim 8 M_{\odot}$  has a Kelvin-Helmholtz time scale that is shorter than a free-fall time scale, therefore it reaches a zero-age main sequence star while mass accretion still occurs.

There exists a basic question how such an MYSO builds its mass against mass ejection by strong stellar wind and expansion of an HII region.

There are two major possible scenarios of massive star formation; the first in term of a massive and thick accretion gas disk/torus and the second in term of lower-mass stars merged into a higher-mass star. In the first scenario, a parent molecular cloud core is still collapsing and providing material into an MYSO with a very high mass-accretion rate (e.g.  $\dot{M} \gtrsim 10^{-3} M_{\odot} \text{ yr}^{-3}$ ) by way of a thick gas disk even if the central part of the core is photoionized (e.g., Keto 2003). The presence of a disk near a massive star can significantly reduce the effect of radiation on the infalling material by reducing the exposure of matter to the radiation field and by allowing photons to escape along the stellar polar axis (e.g. Nagano 1989; Krumholz, McKee, & Klein 2005). A direct evidence for this scenario should be to directly detect mass accretion onto the surface or in very vicinity of an MYSO within  $\sim 1$  AU. Previous observations have reported the existence of such massive disks/tori (e.g. Sako et al. 2005; Jiang et al. 2005; Keto & Wood 2006), but their physical scales directly elucidated by the observations are still much larger ( $>100$  AU). Nevertheless these observations suggested that a single star with a mass at least equal to or lower than  $7 M_{\odot}$  can be created in this scenario (Jiang et al. 2005). The formation mechanism of a higher-mass star is still obscure. Chini et al. (2004) reported an MYSO in M17 with a stellar mass of  $20 M_{\odot}$  and an accompanying massive gas/dust disk, but the estimated mass is reevaluated by Sako et al. (2005) to be only  $3\text{--}8 M_{\odot}$ . In the second scenario, the "runaway collapse" is expected, in which two stars are merged while the third companion is kicked away so that an angular momentum is released by the companion from

this triple star system (e.g., Bonnell, Vine, & Bate 2004; Bonnell & Bate 2006). A massive star is formed as a result of a series of events in which two lower-mass stars are merged. This scenario has been also indirectly supported by observational results, in which an MYSO and other young stellar objects (YSOs) are moving from almost the same position on the sky (in Orion KL/BN region, Rodríguez et al. 2005; Gómez et al. 2005). An explosion may have happened when these stellar objects were located in the common point with strong dynamical interactions (Bally & Zinnecker 2005). However, the stellar volume density requested for this scenario ( $>10^7 \text{ pc}^{-3}$ ) should predict a high frequency of such runaway collapse and explosion events. More observational examples are necessary to widely support this scenario as a major scenario of massive stars.

$\text{H}_2\text{O}$  maser emission is one of the most important probes for study on star formation, often based on data obtained by using very long baseline interferometry (VLBI) with high angular and velocity resolution. Analyses of spatial positions, Doppler velocities, and proper motions of individual maser features with a typical size of 1 AU (Reid & Moran 1981) have revealed the 3-D gas kinematics often in very vicinity ( $\ll 100$  AU) of YSOs (e.g. Claussen et al. 1998; Furuya et al. 2000; Seth et al. 2002; Torrelles et al. 2001; Torrelles et al. 2003; Moscadelli, Cesaroni, & Rioja 2005; Furuya et al. 2005; Goddi et al. 2004; Goddi & Moscadelli 2006). In practice, details of the gas kinematics are complicated but seem to depend on mainly evolutionary status of YSOs.  $\text{H}_2\text{O}$  maser sources sometimes enable us to measure internal motions of giant molecular clouds by measuring relative bulk motions between clusters of  $\text{H}_2\text{O}$  masers that are separated by up to 1 pc but still located within a single antenna

beam (e.g., Imai et al. 2000; Torrelles et al. 2001). Such bulk motions may be owing to, e.g., propagation of shock layers from newly-formed HII regions, cloud contraction by the self-gravitation due to a huge mass of a giant molecular cloud, or runaway motions as mentioned above.

The massive-star forming region G192.16–3.84 (hereafter G192) is located at a distance of  $\sim 2$  kpc, and has massive YSO candidates, one of which is a B2-type star with a giant Herbig-Haro bipolar outflow (Devine et al. 1999) and a possible circumstellar disk (Shepherd, & Kurtz 1999, hereafter SK99; Shepherd, Claussen, & Kurtz 2001, hereafter SCK01; Indebetouw et al. 2003; Shepherd et al. 2004, hereafter SBCSK04). There are two clusters of H<sub>2</sub>O masers separated by  $\sim 0.''6$  ( $\sim 1200$  AU) in the north–south direction (SK99; SBCSK04). The northern and southern clusters exhibit alignments of maser features parallel and perpendicular to two outflows, which are traced by <sup>12</sup>CO emission that are projected roughly in the east–west direction parallel to the Herbig-Haro objects mentioned above (Shepherd et al. 1998, hereafter SWSC98). On the basis of the spatial distribution of H<sub>2</sub>O masers and C<sup>18</sup>O emission tracing high density gas, SK99 and SBCSK04 have proposed that the southern H<sub>2</sub>O maser features are associated with a flattened rotating gas torus around a B2 star, in which the maser velocities are roughly consistent with those in a Keplerian disk.

The Very Long Baseline Array (VLBA) observations of the G192 H<sub>2</sub>O masers were also reported by SBCSK04, but a maser proper motion measurement, especially for the southern cluster of H<sub>2</sub>O masers, was impossible because quenching the maser activity.

Here, we report short-term monitoring observations towards the G192 H<sub>2</sub>O masers with

new Japan VLBI network (JVN, Fujisawa et al. , in preparation), which is newly organized and now consisting of four 20 m telescopes of the VLBI Exploration of Radio Astrometry (VERA), a 45 m telescope of Nobeyama Radio Observatory<sup>1</sup>, a 34 m telescope of Kashima Space Research Center (KSRC), and other 11–64 m dish telescopes in Japan. Fortunately we could detect maser proper motions for both of the maser clusters, leading us to obtaining more direct evidence for the circumstellar disk. Sect. 2 describes the VLBI observations and data reduction. Sect. 3 summarizes analyses of the revealed 3-D kinematics of the H<sub>2</sub>O masers. Sect. 4 discusses the physical conditions and evolutionary statuses of the jet and disk objects in G192.

## 2. Observations and Data Reduction

The VLBI observations were made at three epochs during 2005 March–June, using five or six telescopes of the JVN. Table 1 gives the status of these observations. In each epoch, the observation was made for 8–10 hours including scans of G192 and calibrators (J0530+1331 and DA 193). The received signals were recorded with the SONY DIR1000 recorder with a rate of 128M bits s<sup>-1</sup> and in two base band channels with a band width of 16 MHz each. The VERA telescopes simultaneously observed not only the sources mentioned above but also the position reference source J0603+1742 with the dual beam system (e.g. Honma et al. 2003). The individual base band channels were assigned to observations of either the maser or reference source.

The data correlation was made with the Mitaka FX correlator (Chikada et al. 1991).

---

<sup>1</sup> NRO and VERA observatory are branches of the National Astronomical Observatory, an interuniversity research institute operated by the Ministry of Education, Culture, Sports, Science and Technology.

An accumulation period of the correlation was set to 1 s. The correlation outputs consisted of 1024 velocity channels, each of which has a velocity spacing of  $0.21 \text{ km s}^{-1}$ . From the VERA telescopes, there were two correlation outputs including scans of G192 and the calibrators in the first and the reference source in the second, respectively.

Data reduction to obtain image cubes for the maser source was made with the NRAO AIPS package in normal procedures (e.g., Diamond 1995). Fringe fitting and self-calibration procedures were made for a Doppler velocity channel including a bright maser spot (velocity component) in G192, which is also given in Table 1. The solutions were applied to all of the data in other velocity channels. A typical size of the synthesized beam was 1 milliarcseconds (mas) in the three observations (see Table 1). A relative position accuracy of a maser spot was ranged in 0.01–0.09 mas depending on a signal-to-noise ratio and spatial structure of the spot. Identification of an  $\text{H}_2\text{O}$  maser feature (a cluster of maser spots or velocity components) was made in the same procedure shown in several previous papers (e.g. Imai et al. 2000), in which the feature position is defined as a brightness peak in the feature. A relative position accuracy of a maser feature was ranged in 0.03–0.17 mas. Relative proper motions were measured for maser features identified at least at two of the three epochs.

The position reference source J0603+1742 was marginally but reliably detected at only the first epoch with the *inverse phase-referencing technique*, in which fluctuation of visibility phases in the J0603+1742 data were compensated by those in the spectral channel (see the phase-reference velocity channel shown in table 1) that included the brightest maser emission in the feature G192.16–3.84:J2006 9. J0603+1742 had a correlated peak intensity of

50 mJy beam<sup>-1</sup> with a beam tapered by a  $uv$ -distance of 80 M $\lambda$ .

### 3. Results

#### 3.1. Summary of the revealed maser spatio-kinematical structure

Table 1 shows the numbers of the detected H<sub>2</sub>O maser features in the G192 region. Although the H<sub>2</sub>O maser emission in G192 is highly time-variable, we could detect most of velocity components found in the previous VLA/VLBA observations (SK99; SBCSK04). *Relative* proper motions of eight maser features with respect to the maser feature G192.16–3.84:J2006 1 (see table 2) as position reference were identified. Table 2 lists the measured proper motions. Figure 1 shows time variations of positions and Doppler velocities of the maser features that are detected their relative proper motions.

We found a flow such as a highly-collimated bipolar jet in the maser spatio-kinematical structure in the northern maser cluster. We estimated a bias of the proper motion vectors with respect to the intrinsic motion of the position-reference feature,  $(\bar{V}_x, \bar{V}_y) = (23, -34)$  [km s<sup>-1</sup>], by calculating a mean of two velocity vectors that are equally-weighted average proper motions of the NE and SW clusters of maser features, respectively, in the northern cluster. Figure 2 shows the distribution and the relative proper motion fields of H<sub>2</sub>O masers in G192, in which the proper motion vectors are subtracted by the velocity bias so that a systemic motion of the northern jet is removed. A Doppler velocity bias, likely corresponding to the systemic radial velocity of the source driving the maser jet is about  $V_{\text{LSR}} = 5$  km s<sup>-1</sup>, which is consistent with the systemic velocity of the CO molecular outflow seen on a much larger scale in roughly the same direction within 1 km s<sup>-1</sup> (e.g., Snell et al. 1990; SK99).



Fortunately, we also detected two maser features  $\sim 1200$  AU away from the bipolar jet with Doppler velocities  $V_{\text{LSR}} = -6.8 \text{ km s}^{-1}$  and  $16.0 \text{ km s}^{-1}$  (G192.16–3.84:J2006 1 and 9, hereafter abbreviated as the features A and B, respectively). The both features are moving toward the bipolar jet, but the feature B is relatively receding by  $\sim 10 \text{ km s}^{-1}$  in the SSW direction with respect to the feature A. The positions and the relative proper motion of the two features provide strong constraints on kinematical models of the masers discussed in Sect. 3.6, 3.5.

### 3.2. Astrometry for the $\text{H}_2\text{O}$ maser source

As described in Sect. 2, we successfully detected the position reference source J0603+1742 to obtain the absolute coordinates of the G192.16–3.84  $\text{H}_2\text{O}$  masers. Based on the measured coordinate offsets of J0603+1742 with respect to its true coordinates, we estimated coordinates of the maser feature B to be, R.A.(J2000.0)= $05^{\text{h}}58^{\text{m}}13^{\text{s}}.5332$ , decl.(J2000.0)=  $+16^{\circ}31'58''.483$ . Taking into account difference in the coordinates obtained by some data analyses adopting different analyzing parameters, an uncertainty of the measured coordinates is expected to be about 6 mas. This accuracy is still much worse than those achieved by the latest results of VERA astrometry (Honma et al. , Hirota et al. , and Imai et al. in 2006, in paper preparation), but does not affect any interpretation in the present paper.

This astrometry enables us to superpose the  $\text{H}_2\text{O}$  maser maps made from previous VLA/VLBA and our JVN observations with an accuracy better than 100 mas. Our  $\text{H}_2\text{O}$  maser maps can be superposed on the 7 mm continuum map with an accuracy of about 20 mas. These accuracies are estimated from the astrometric accuracies of previous VLA observations

(SCK01; SBCSK04) and uncertainty of a secular motion of the maser source due to the Galactic rotation and an unknown local motion. The maser features A and B were located closest to the positions of the maser features detected by SK99 at a Doppler velocity  $V_{\text{LSR}} \simeq 10 \text{ km s}^{-1}$ . The superposed distribution of the  $\text{H}_2\text{O}$  masers together with relative proper motions reveals more clearly the kinematics of the  $\text{H}_2\text{O}$  masers in the northern and southern clusters.

### 3.3. *Objective analyses of the jet kinematics for the northern maser cluster*

In order to objectively or model-independently find an axis of a jet accompanying the northern maser cluster, we performed diagonalization for the velocity variance–covariance matrix (VVCM) obtained from velocity vectors of maser features (c.f., Bloemhof 2000). The eigenvector corresponding to the largest eigenvalue (velocity dispersion) indicates a major axis of the jet. A square root of the largest and second largest eigenvalue gives a collimation factor of the jet. Uncertainties of the obtained eigenvectors and eigenvalues were derived from standard deviations of these parameters, which were calculated by the Monte–Carlo simulation for the VVCM diagonalization using velocity vectors randomly distributed around the observed values within their estimated errors. Table 3 gives the obtained eigenvalues and their corresponding eigenvectors after the matrix diagonalization. In the cases of G192, the eigenvector corresponding to the largest eigenvalue has an inclination of  $2^\circ$  with respect to the sky plane and a position angle of  $60^\circ$  east from the north. This vector is almost parallel to outflows found in the Herbig-Haro objects and  $^{12}\text{CO}$  emission on a much larger scale. Proper motions with a systemic velocity bias subtracted (see figure 2) are also roughly parallel to this vector. These suggest that the maser jet and the CO outflow should be in the same outflow without

significant precession.

Similar to the VVCM, the spatial variance–covariance matrix is obtained from the maser feature distribution, which also gives an eigenvector direction similar to that of the major axis for the VVCM. Taking into account a velocity collimation factor of 4.9 and the bipolarity of the velocity vectors, the maser spatio-kinematical structure indicates a highly-collimated bipolar jet. Note that maser velocity vectors in the south-west cluster in the bipolar jet are directed toward both directions of the bipolar jet. This maser cluster also contains both of the red-shifted and the blue-shifted maser components in the maps obtained by SBKSC04. Note that the large scale molecular outflows are estimated to be driven by the southern YSO having the southern maser cluster, not by the northern YSO having this northern maser cluster (SWSC98; Devine et al. 1999). The VVCM analysis for the H<sub>2</sub>O masers suggests that there are two outflows in G192.16–3.84 that are parallel, one of which is highly collimated and almost completely parallel to the maser jet.

#### *3.4. Dynamical ages of the bipolar outflows in G192.16–3.84*

We estimated dynamical ages of the bipolar outflows driven by the northern and southern YSOs in G192 on basis of the 3-D kinematical structure of the H<sub>2</sub>O masers that are associated with the outflow driven by the northern object (see sect. 3.1). The outflow found in the Herbig-Haro objects and <sup>12</sup>CO emission is likely to be driven by the southern object (SWSC98) and the outflow driven by the northern object may not directly seen on the same scale. Nevertheless the latter is expected to be included in the <sup>12</sup>CO emission and to have a length equal to or shorter than that of the former. The <sup>12</sup>CO emission flow also extends in the north–south directions

by  $\sim 0.6$  pc and seems to have two axes of outflows with similar projected lengths. One of the outflow axes might trace the outflow driven by the northern YSO. If the northern and southern objects started their star formation process from a common molecular cloud core, these outflows may simultaneously ignite and have the same dynamical age, and eventually roughly the same outflow velocity.

The length of the southern outflow projected on the sky is estimated to be  $\sim 5.7$  pc from the existence of the Herbig-Haro objects HH396/397 (Devine et al. 1999, see also the  $^{12}\text{CO}$  emission map of SWSC98). This length is an upper limit of that of the northern outflow. On the other hand, the velocity of the northern outflow is estimated to be  $\sim 100$  km s $^{-1}$  in the present work from the blue-shifted maser feature G192.16–3.84:J2006 7 that is moving fastest from the vicinity of the flow’s kinematical center (see figure 2). Therefore, assuming a constant velocity in the whole outflow, a dynamical age of the outflows is about  $5.6 \times 10^4$  yrs. This value is shorter by a factor of 3.5 than those previously estimated without any information of the 3-D flow velocity ( $\sim 2 \times 10^5$  yrs, Snell et al. 1990; SWSC98; Devine et al. 1999).

### 3.5. *A relative bulk motion between the northern and southern maser clusters in G192.16–3.84*

In the present work, we clearly detected a relative bulk motion, in which the northern and southern clusters of H $_2$ O masers are approaching each other by  $\sim 40$  km s $^{-1}$ . Figure 2 shows that in this velocity the features A and B are approaching the northern maser cluster whose systemic motion is removed in this figure (see sect. 3.1). If the YSO located at the dynamical center of the northern outflow is close to the south-west cluster of maser cluster as mentioned in sect. 3.1, the direction of the bulk motion is exactly along the alignment of the

two YSOs. Thus it is possible that these two YSOs might be dynamically linked. However the approaching speed is extraordinary large and it is unlikely that this bulk motion is an orbiting motion between the two YSO. When supposing this motion as an orbiting motion, a possible lower limit of an enclosed mass in this system should be as large as  $1700 M_{\odot}$ , such a huge mass within such a small scale ( $\sim 1200$  AU) has never been observed in this region. On the other hand, the systemic velocities of the two YSO may be almost equal within  $1 \text{ km s}^{-1}$  as mentioned in sect. 3.1 and 3.6. Therefore, a true relative bulk motion between the two YSOs should be much smaller, about  $2\text{--}3 \text{ km s}^{-1}$ , which corresponds to an enclosed mass of about  $10 M_{\odot}$  in this system.

The possible existence of an outflow parallel to the relative maser bulk motion may also be rejected. The  $\text{H}_2\text{O}$  maser features associated with the southern YSO and detected by previous and present works are aligned over  $1000$  AU. in the north–south direction. The alignment is also parallel to that found in  $\text{C}^{18}\text{O}$  emission on an angular scale of  $10000$  AU (SK99). The dynamical center of the masers should be one of the continuum emission sources detected in  $3.6 \text{ cm}$ ,  $1.3 \text{ cm}$ ,  $7 \text{ mm}$ , and  $2.6 \text{ mm}$  bands, which are located within  $\sim 400$  AU from the masers. It is impossible to form a straight alignment of masers longer than this scale by a shock wave front created by an outflow driven perpendicular to the alignment. A major axis of a (highly-collimated) outflow might exist along this alignment. However, the distributions of Herbig-Haro objects and  $^{12}\text{CO}$  emission indicate the existence of outflows only in the roughly east–west direction (SWSC98; Devine et al. 1999). It is unreasonable to interpret that only  $\text{C}^{18}\text{O}$  emission is detected in the north–south direction as a tracer of a high density outflow.

$^{13}\text{CO}$  emission mapped by SWSC98 may trace expanding shells created along the interface between the outflow and ambient cloud gas. The opening angle of the shells from the axis is  $45^\circ$  and one of the shells is aligned roughly parallel to the direction of the maser bulk motion. However, the observed bulk motion is much faster than the shell expansion ( $\sim 8 \text{ km s}^{-1}$ ). Except for the possibility of a binary system in the southern YSO itself, it is most feasible to interpret that the measured relative maser bulk motion should be coming from another internal motions of the maser features, such as motions expected from a rotating disk model discussed in the next section.

### *3.6. An infalling-rotating thin disk model for the southern YSO*

The previous VLBA and VLA observations (SK99; SBCSK04) have detected more than 10  $\text{H}_2\text{O}$  maser features in the southern cluster of features and found the maser alignment in the north–south direction, which is roughly parallel to those of the elongated morphology and a velocity gradient seen in  $\text{C}^{18}\text{O}$  emission (SK99). SK99 found a clearer velocity gradient in the maser distribution and fitted it to a model of a Keplerian rotating gas disk whose center is located around the peak of 7 mm/3.6 cm continuum emission in G192.16–3.84, or likely a B-type YSO. Later SBCSK04 found maser components with significant red shift ( $11 \geq V_{\text{LSR}} \geq 15 \text{ km s}^{-1}$ ) in the east side of the maser alignment found by SK99, which is inconsistent with the locations expected from a bipolar outflow in the east–west direction with an opposite velocity gradient (SWSC98) or another possible outflow parallel to the maser alignment. Such a complicated maser distribution may be explained by combination of outflow, infall, and rotation motions.

Here we attempt to obtain a spatio-kinematical model for the H<sub>2</sub>O masers detected in the previous and present observations. We adopt a disk model proposed by Cassen & Moosman (1981) and Fiebig (1997), in which gas clumps are moving in the trajectory planes with a specific angle with respect to the axis perpendicular to the disk and impinging onto the disk. H<sub>2</sub>O maser emission is expected to be excited on the disk where an infalling gas clump collides with the disk and reaches an appropriate physical condition for maser excitation ( $T \simeq 400$  K and  $n_{\text{H}_2} \simeq 10^9 \text{ cm}^{-3}$ ) by shock. The velocity field of the disk ( $v_r, v_\theta, v_\phi$ ) is calculated using the zero-energy orbits of the impinging clumps on parabolas, and is expressed in the spherical coordinate system as follows,

$$v_r = -\left(\frac{GM_*}{r}\right)^{1/2} \quad (1)$$

$$v_\theta = \left(\frac{GM_*}{r}\right)^{1/2} \cos \theta_0 \quad (2)$$

$$v_\phi = \left(\frac{GM_*}{r}\right)^{1/2} \sin \theta_0 \quad (3)$$

$$\sin^2 \theta_0 = r/r_{\text{d}}. \quad (4)$$

Here  $r$  is the distance from the central object on the disk,  $M_*$  the mass of the central stellar object,  $\theta_0$  the angle between the disk rotation axis and the trajectory plane of the clump, and  $r_{\text{d}}$  the distance from the stellar object where  $\theta_0 = 0$ . Note that the velocity component  $v_\theta$  should be zero for the clump on the disk with maser emission excited after collision with the disk. To examine the disk model proposed previously, we adopt physical parameter values that are similar to those estimated previously. A systemic velocity of  $V_{\text{LSR}} = 5.7 \text{ km s}^{-1}$  assumed here is estimated from the C<sup>18</sup>O and NH<sub>3</sub> emission detected with radio interferome-

ters (SK99; SBCSK04). A disk inclination with respect to the line of sight is estimated to be  $\theta \simeq 63^\circ$  (SWSC98; SK99). An outer disk radius  $r_d$  may be equal to or smaller than 1000 AU ( $0''.5$  at 2 kpc), this upper limit corresponds to a separation between the northern and southern clusters of the H<sub>2</sub>O masers.

Through several trials of the model fitting, we have found that a position angle of the disk axis, P.A.=60–75° east from the north, and a stellar mass of 5–10  $M_\odot$  provides a model consistent with the observed 3-D maser kinematical structure. These two parameters estimated are consistent with those previously suggested ( $\sim 75^\circ$  and 6–10  $M_\odot$ , respectively, SK99; SCK01). Figure 3 shows the spatial distribution of maser Doppler velocities which are expected in one of the best consistent model. Although figure 3 shows the distribution of only the H<sub>2</sub>O masers detected by the present observations, the proposed model (figure 3*a* and *b*) may well explain the Doppler velocity distribution of the maser features that have been detected both by previous and present works. The modeled radial velocity field is also roughly consistent with that found in C<sup>18</sup>O emission, exhibiting a velocity gradient in the north-south direction on the scale larger than 2000 AU (SK99).

One exception in the consistency is the maser feature at  $V_{\text{LSR}} \simeq -7 \text{ km s}^{-1}$  that was located in the southern part of the southern maser cluster and detected with the VLA (SWSC98; SBCSK04) with a big position uncertainty. The maser clusters exhibit a velocity gradient in the NNW–SSE direction, but its direction is inversed at the vicinity of the peak of continuum emission (SBCSK04). Such a complicated velocity distribution cannot be explained by either a pure Keplerian rotation disk (figure 3*d*) or a bipolar outflow as mentioned above.



Furthermore, a relative proper motion of two maser features, A and B with (see table 2), in the southern cluster detected in the present work is also consistent with that expected by this model. The vector of the relative motion is roughly consistent with that expected from the model (by  $\sim 10 \text{ km s}^{-1}$  in the SSE direction), in which the feature B is located much closer to the dynamical center of the disk than the feature A. This relative motion does not appear in a purely Keplerian rotation model (figure 3d) because the two maser features are located at almost an equal distance from the dynamical center and the two proper motion vectors are also almost equal. The proposed model is also supported by a mean bulk motions of the two maser features with respect to the northern maser cluster mentioned in sect. 3.5.

Note that the dynamical center of the modeled disk proposed in the present work is located at the *north* of the two maser features,  $\sim 0''.2$  north from the peaks of 3.6 cm and 7 mm continuum emission SCK01, or closer to a peak of 2.6 mm continuum emission (SK99). When the dynamical center is put in the south of the two maser features or closer to the peaks of 3.6 cm and 7 mm continuum emission as shown in figure 3c, an extraordinary fast ( $\sim 60 \text{ km s}^{-1}$ ) bulk motion of the YSO with respect to the northern cluster of H<sub>2</sub>O maser features appears. However, it is still obscure whether these continuum emission peaks indicate a single YSO or a YSO binary.

## 4. Discussion

### 4.1. *The physical condition on the infalling-rotating disk in the G192.16–3.84 southern YSO*

On a disk proposed in the present paper, it receives gas clumps that are impinging on the disk and exciting H<sub>2</sub>O maser emission by the shock. The physical condition that can excite the

maser emission is described in detail by Fiebig (1997). This paper demonstrates the existence of a disk traced by H<sub>2</sub>O maser emission in IRAS00318+6312 (L1287). On the L1287 disk, a pre-shock gas density, a mass of the central YSO, and an outer disk radius are estimated to be  $n_{\text{H}_2} \geq 10^4 \text{ cm}^{-3}$  and  $3 M_{\odot}$ , and  $r_{\text{d}} = 4500 \text{ AU}$ , respectively. The H<sub>2</sub>O maser emission is excited within 35 AU from the YSO, where an impinging gas clump collides with the disk with an impact velocity  $V_{\theta} \geq 3.1 \text{ km s}^{-1}$  (see eq. 4) to be heated over 400 K. A gas density at least equal to that in the L1287 disk is expected for the disk in the G192 disk from the detection of C<sup>18</sup>O and NH<sub>3</sub> emission (SBCSK04). In the same gas density as that in L1287 but a higher central mass of  $\sim 8 M_{\odot}$  and a smaller disk radius ( $r_{\text{d}} \leq 1000 \text{ AU}$ ) for G192, a radius of maser excitation is expected to be 420 AU ( $\sim 0''.21$ ). This radius roughly covers the whole region of the maser emission detected with the VLA (SK99; SBCSK04).

Note that the proposed disk model is very thin but still consistent with a thick disk/torus model (SCK01) because H<sub>2</sub>O maser may be excited at the mid-plane of the disk/torus with the highest gas density ( $n_{\text{H}_2} = 10^9 - 10^{11} \text{ cm}^{-3}$ , Elitzur, Hollenbach, & McKee 1989).

#### 4.2. *A mass accretion on the circumstellar disk and a massive gas disk scenario for massive-star formation*

On basis of the proposed disk model for the H<sub>2</sub>O maser kinematics, a rate of mass accretion on the circumstellar disk is derived as follows,

$$\begin{aligned} \dot{M}_{\text{disk}}[M_{\odot}\text{yr}^{-1}] &= \int_0^{r_{\text{d}}} 2\pi r v_{\theta} \rho dr \\ &\simeq 1.6 \times 10^{-7} [n_{\text{H}_2}/10^4 \text{ cm}^{-3}] [M_{*}/8 M_{\odot}]^{1/2} [r_{\text{d}}/1000 \text{ AU}]^{3/2}, \end{aligned} \quad (5)$$

where  $n_{\text{H}_2}$  is the gas density of the impinging gas clumps, or equal to a pre-shock gas density of a

maser clump. When assuming a pre-shock gas density  $n_{\text{H}_2} \geq 10^4 \text{ cm}^{-3}$  adopted by Fiebig (1997), the obtained accretion rate is much smaller than a mass loss and infall rates previously estimated,  $5.6 \times 10^{-4} M_{\odot} \text{ yr}^{-1}$  and  $\sim 10^{-5} M_{\odot} \text{ yr}^{-1}$ , respectively (SK99; SCK01). Note that this disk is an inner part of the region with  $\text{C}^{18}\text{O}$  emission tracing dense gas  $n_{\text{H}_2} \geq 10^{-4} \text{ cm}^{-3}$  (SK99) and that maser excitation models request a much higher pre-shock gas density ( $n_{\text{H}_2} \sim 10^7 \text{ cm}^{-3}$ , Elitzur, Hollenbach, & McKee 1989). Adopting this density, we obtained a accretion rate of  $\sim 1.6 \times 10^{-4} M_{\odot} \text{ yr}^{-1}$ . To obtain the accretion rate equal to that previously estimated, a higher density,  $n_{\text{H}_2} \geq 6 \times 10^5 \text{ cm}^{-3}$  is expected.

If an estimated accretion rate has persisted since the earliest phase of the star formation in G192, total accreted masses for above two accretion rates give  $10 M_{\odot}$  and  $0.6 M_{\odot}$ , respectively. The upper estimated value supports a recent conclusion that a massive gas disk scenario for forming a massive star is applicable to a stellar object as massive as  $\sim 7 M_{\odot}$  (Sako et al. 2005; Jiang et al. 2005). It is also possible to increase in the mass accretion rate at the younger age and to lose a stellar mass due to the outflow. Therefore, it is still difficult for such stellar mass estimation in order to flag proposed scenarios of massive star formation performed in G192.

Note that a scenario in which multiple YSOs merge into a massive star is not completely ruled out yet in G192. The existence of a disk with active accretion and a developed outflow in G192 indicates that these have been continuously developed since their birth without their disruption by any merger event (Rodríguez et al. 2005). However, SCK01 and the present work suggest the existence of more than one YSO near the disk center. If these stars are

gravitationally bound, they might merge in the near future. Such a merger scenario may be applicable to a YSO with a mass equal to or larger than those discussed above ( $M \geq 10 M_{\odot}$ ).

#### 4.3. *Evolutionary stages of two outflows and two YSOs in G192.16–3.84*

Because the northern and southern YSOs are located within 1600 AU and have systemic radial velocities equal within  $1 \text{ km s}^{-1}$  ( $V_{\text{LSR}} \simeq 6 \text{ km s}^{-1}$ ), they should be associated with the same parental molecular cloud. SCWC98, SK99, SCK01, and SBCSK04 have demonstrated that the southern YSO is a B2-type star while the northern YSO is a lower mass star on the basis of a kinematic energy of the  $^{12}\text{CO}$  emission outflow and a luminosity of each star estimated from the continuum emission, which are correlated each other. Properties of the flux density variation and the spatio-kinematics of  $\text{H}_2\text{O}$  masers also may indicate some properties or the evolutionary status of their driving stellar objects.  $\text{H}_2\text{O}$  masers associated with MYSOs tend to have less-collimated spatio-kinematical structures (Imai et al. 2000; Torrelles et al. 2001; Torrelles et al. 2003; Moscadelli, Cesaroni, & Rioja 2005; Goddi et al. 2004; Goddi & Moscadelli 2006, and references therein), while those associated with some lower-mass YSOs at the very early stage have highly-collimated ones. (Claussen et al. 1998; Furuya et al. 2000; Seth et al. 2002; Furuya et al. 2005, and references therein). A luminosity of  $\text{H}_2\text{O}$  masers associated with an MYSO seems to be higher and temporally more stable than that associated with a low-mass YSO. Note that  $\text{H}_2\text{O}$  masers in W75N exhibit quite different spatio-kinematics although the radio continuum emission properties of their driving stellar objects are quite similar (Torrelles et al. 2003). It implies that the maser spatio-kinematical structure also evolves as the accompanying YSO and its outflow evolve within a period ( $t \lesssim 10^4 \text{ yrs}$ ) shorter

than duration of H<sub>2</sub>O maser emission in the same source ( $t \lesssim 10^5$  yrs, Genzel & Downes 1977).

The spatio-kinematical structure of the H<sub>2</sub>O masers associated with the northern YSO in G192 is highly-collimated as described in §3. A luminosity of these masers is higher and temporally more stable than that in the southern YSO in G192. However our unpublished single-dish spectral data of the H<sub>2</sub>O masers in G192 shows rapid and significant time variation in the maser luminosity as shown in the masers associated with low-mass YSOs. Therefore we also suggest that the northern YSO in G192 is a lower mass than the southern YSO (B2 star). On the other hand, the H<sub>2</sub>O masers associated with the southern YSO is tracing an infalling-rotating thin disk, perfectly different from those associated with the northern YSO. The southern YSO may be different in the stellar mass and the evolutionary status from the northern YSO.

Shepherd (2005) (see also references therein) discusses the evolution of outflow morphology with the evolution of a massive YSO. In the evolutionary scenarios, two sequences of the massive star evolution are considered, in the first from a high-mass protostellar object (HMPO) via a hyper-compact (HC) HII region to a ultra-compact (UC) HII region, and in the second an O-type star evolves from a B-type star then reaches its final mass and stellar luminosity. In both of the sequences, an outflow gets less collimated with its evolution. Duration of above evolution may be roughly  $10^4$  yrs (Shepherd 2005), consistent with that expected from the difference in maser spatio-kinematics proposed by Torrelles et al. (2003). In G192, the southern YSO is expected to more evolve because of the existence of a more developed HII region (SBCSK04) and the absence of high collimation of the outflow. Note that mass accre-

tion should still persist in the southern YSO through a gas disk that may be thinner than that possibly existing around the northern YSO. However, 7 mm continuum emission is detected in only southern YSO (SBCYK04), suggesting enrichment of gas and dust around the southern YSO and the earlier stage of the YSO. Taking into account the difference in stellar mass and evolution speed, it is concluded that within the same dynamical age, the southern YSO with a higher mass evolves more rapidly and its highly-collimated jet with H<sub>2</sub>O maser excitation disappear sooner than the northern YSO. The clearer conclusion of the evolutionary status of these YSOs requests information of the gas/dust distribution and the jet morphology in higher angular resolution ( $\leq 0''.1$ ).

## 5. Conclusions

We have obtained data of the three-dimensional kinematics of H<sub>2</sub>O masers in G192 with short-term ( $\sim 2$  months) VLBI monitoring observations, which were made with the JVN during 2005 March–June, in different epochs from those previously made with the VLA and the VLBA (SBCSK04). The H<sub>2</sub>O masers are associated with two MYSOs, which have a highly collimated jet and an infalling-rotating gas disk and located at the northern and southern parts in G192, respectively. We have obtained stronger evidence than obtained by previous observations for the existence of an infalling-rotating disk with a radius of  $\sim 1000$  AU and a central stellar mass of 5–10  $M_{\odot}$ . The absence of any molecular outflow along the maser alignment found in the previous VLA observation (SK99) may reject the possibility that there exists a jet or an equatorial flow perpendicular to the observed molecular outflow with a total length of 5.7 pc. On the basis of the spatio-kinematical structure of the jet traced by H<sub>2</sub>O maser and <sup>12</sup>CO

emission as well as assumption of the same dynamical age of the jet and the disk, we estimated a dynamical age of the jet/disk system in G192 to be about  $5.6 \times 10^4$  yrs. With an assumed gas clump density appropriate for maser excitation, we have speculated that a massive YSO with a mass of  $\sim 8 M_{\odot}$  has an accretion disk that has provided the material onto the YSO with a rate of  $10^{-7} - 10^{-5} M_{\odot} \text{yr}^{-1}$ . These partially supports a massive accretion scenario for massive star formation. However, there still exist possibility that this massive YSO will become a higher-mass star by merging with a lower-mass YSO. Observations so as to more clearly elucidate the spatio-kinematics of the  $\text{H}_2\text{O}$  masers and to directly estimate the pre-shock gas density are crucial for estimating a total mass of the existing massive YSO and destiny of the object. They also should provide clues for elucidating a history of mass accretion and outflow.

We acknowledge all staff members and students who have helped in array operation and in data correlation of the JVN/VERA. H. I. and T. H. were supported by Grant-in-Aid for Scientific Research from Japan Society for Promotion Science (16540224).

## References

- Bally, J., & Zinnecker, H. 2005, *AJ*, 129, 2281
- Bloemhof, E. E. 2000, *ApJ*, 533, 893
- Bonnell, I. A., & Bate, M. R. 2006, *MNRAS*, in press (astro-ph/0604615)
- Bonnell, I. A., Vine, S. G., & Bate, M. R. 2004, *MNRAS*, 349, 735
- Cassen, P., & Moosman, A. 1981, *Icarus*, 48, 363
- Chini R., Hoffmeister, V., Kimeswenger, S., Nielbock, M., Nürnberg, D., Schmidtobreick, L., & Sterzik, M. 2004, *Nature*, 429, 155
- Chikada, Y., Kawaguchi, N., Inoue, M., Morimoto, M., Kobayashi, H., Mattori, S., Nishiura, T., Hirabayashi, H. et al. 1991, in *Frontiers of VLBI*, ed. H. Hirabayashi, M. Inoue, & H. Kobayashi (Tokyo: Universal Academy Press), p. 79
- Claussen, M. J., Marvel, K. B., Wootten, A., & Wilking, B. A. 1998, *ApJ*, 507, L79
- Devine, D., Bally, J., Reipurth, B., Shepherd, D. S., & Watson, A. M. 1999, *AJ*, 117, 2919
- Diamond, P. J. 1995, in *ASP Conf. Ser. 82, VERY LONG BASELINE INTERFEROMETRY AND THE VLBA*, ed. J. A. Zensus, P. J. Diamond, & P. J. Napier (San Francisco: ASP), p. 227
- Elitzur, M., Hollenbach, D. J., & McKee, C. F. 1989, *ApJ*, 346, 983
- Fiebig, D. 1997, *A&A*, 327, 758 (F97)
- Furuya, R. S., Kitamura, Y., Wootten, H. A., Claussen, M. J., & Kawabe, R. 2005, *A&A*, 438, 571
- Furuya, R. S., Kitamura, Y., Wootten, H. A., Claussen, M. J., Saito, M., Marvel, K. B., & Kawabe, R. 2000, *ApJ*, 542, L135
- Genzel, R., & Downes, D. 1977, *A&AS*, 30, 145
- Goddi, C., & Moscadelli, L., 2006, *A&A*, 447, 587
- Goddi, C., Moscadelli, L., Alef, W., & Brand, J. 2004, *A&A*, 420, 929
- Gómez, L., Rodríguez, L. F., Loinard, L., & Lizano, S. 2005, *ApJ*, 635, 1166
- Honma, M., Fujii, T., Hirota, T., Horiai, K., Iwadate, K., Jike, T., Kameya, O., Kamohara, R., et al. 2003, *PASJ*, 55, L57
- Imai, H., Iwata, T., & Miyoshi, M. 1999, *PASJ*, 51, 473
- Imai, H., Kameya, O., Sasao, T., Miyoshi, M., Deguchi, S., Horiuchi, S., & Asaki, Y. 2000, *ApJ*, 538, 751
- Indebetouw, R., Watson, C., Johnson, K. E., Whintney, B., & Churchwell, E. 2003, *ApJ*, 596, L83
- Jiang, Z., Tamura, M., Fukagawa, M., Hough, J., Lucas, P., Suto, H., Ishii, M., & Yang, J. 2005, *Nature*, 437, 112
- Keto, E., & Wood, K. 2006, *ApJ*, 637, 850
- Keto, E. 2003, *ApJ*, 599, 1196
- Krumholtz, M. R., McKee, C. F., & Klein, R. I. 2005, *ApJ*, 618, L33
- Moscadelli, L., Cesaroni, R., & Rioja, M. J. 2005, *A&A*, 438, 889
- Nagano, T. 1989, *ApJ*, 345, 464
- Reid, M. J., & Moran, J. M. 1981, *ARA&A*, 19, 231
- Rodríguez, L. F., Poveda, A., Lizano, S., & Allen, C. 2005, *ApJ*, 627, L65
- Sako, S., Yamashita, T., Kataza, H., Miyata, T., Okamoto, Y. K., Honda, M., Fujiyoshi, T., & Terada, H., et al. . 2005, *Nature*, 434, 995



- Seth, A. C., Greenhill, L. J., & Holder, B. P. 2002, *ApJ*, 581, 325
- Shepherd, D. 2005, in IAU symposium 227, eds. R. Cesaroni, M. Felli, E. Churchwell & M. Walmsley (Cambridge: Cambridge Univ. Press), p. 237
- Shepherd, D. S., Borders, T., Claussen, M. J., Shirley, Y. & Kurtz, S. E. 2004, *ApJ*, 614, 211 (SBCSK04)
- Shepherd, D. S., Claussen, M. J., & Kurtz, S. E. 2001, *Science*, 292, 1513 (SCK01)
- Shepherd, D. S., & Kurtz, S. E. 1999, *ApJ*, 523, 690 (SK99)
- Shepherd, D. S., Watson, A. M., Sargent, A. I., & Churchwell, E. 1998, *ApJ*, 507, 861 (SWSC98)
- Snell, R. L., Dickman, R. L., & Huang, Y.-L. 1990, *ApJ*, 352, 139
- Torrelles, J. M., Patel, N. A., Anglada, G., Gómez, J. F., Ho, P. T. P., Lara, L., Alberdi, A., Cantó, J., et al. 2003, *ApJ*, 598, L115
- Torrelles, J. M., Patel, N. A., Gómez, J. F., Ho, P. T. P., Rodoriguez, L. F., Anglada, G., Garay, G., & Greenhill, L. J., et al. 2001, *ApJ*, 560, 853

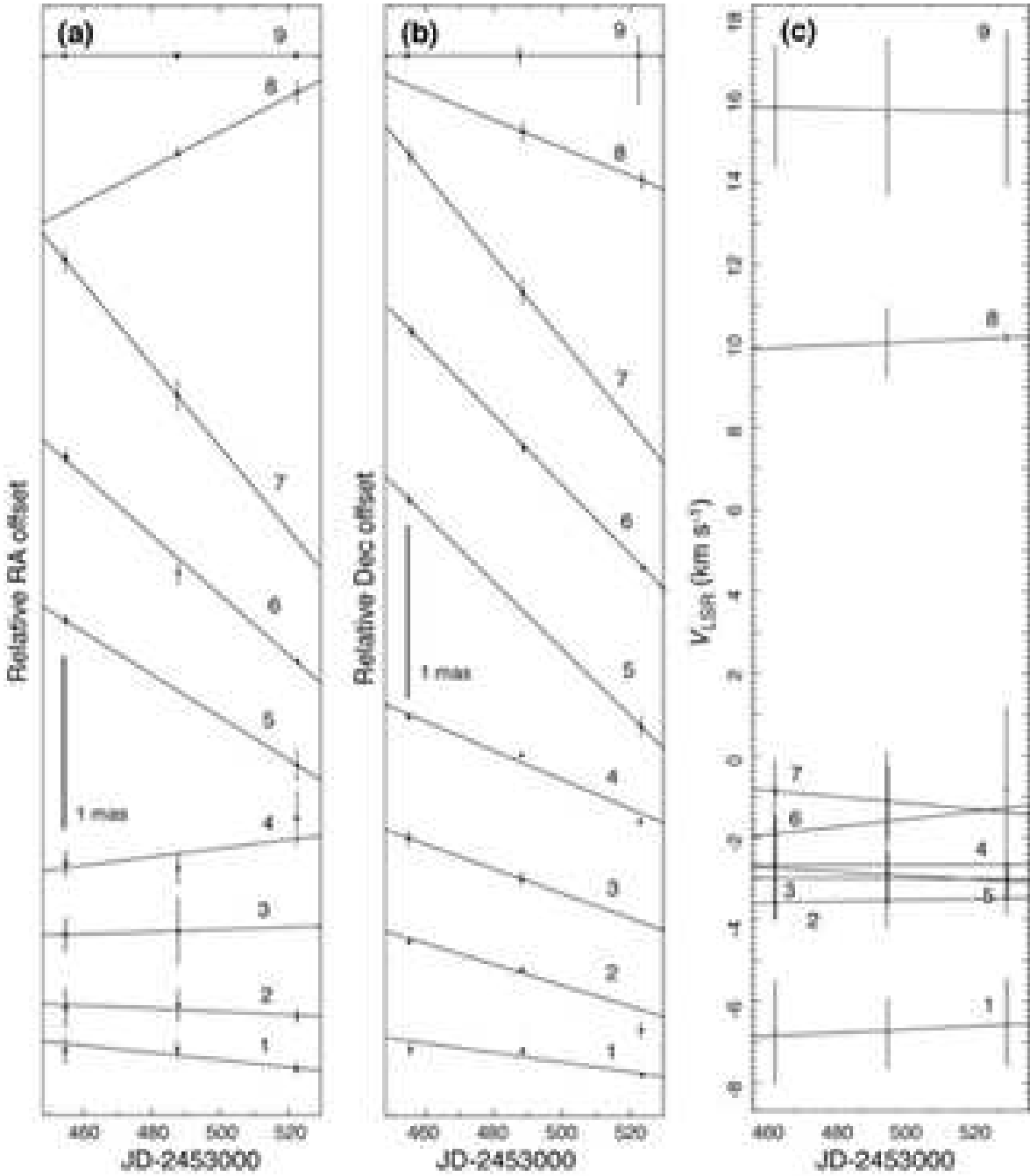


**Fig. 1.** Observed relative proper motions (sub-panels a and b) and Doppler velocity variations (sub-panel c) of H<sub>2</sub>O maser features in G192.16–3.84. A number added for each feature in each sub-panel shows the assigned one after the designated name form “G192.16–3.84: I2006”. A solid line in the position or Doppler velocity plot indicates a least-square-fitted line assuming a constant velocity motion in the proper motion or a constant Doppler velocity drifts.

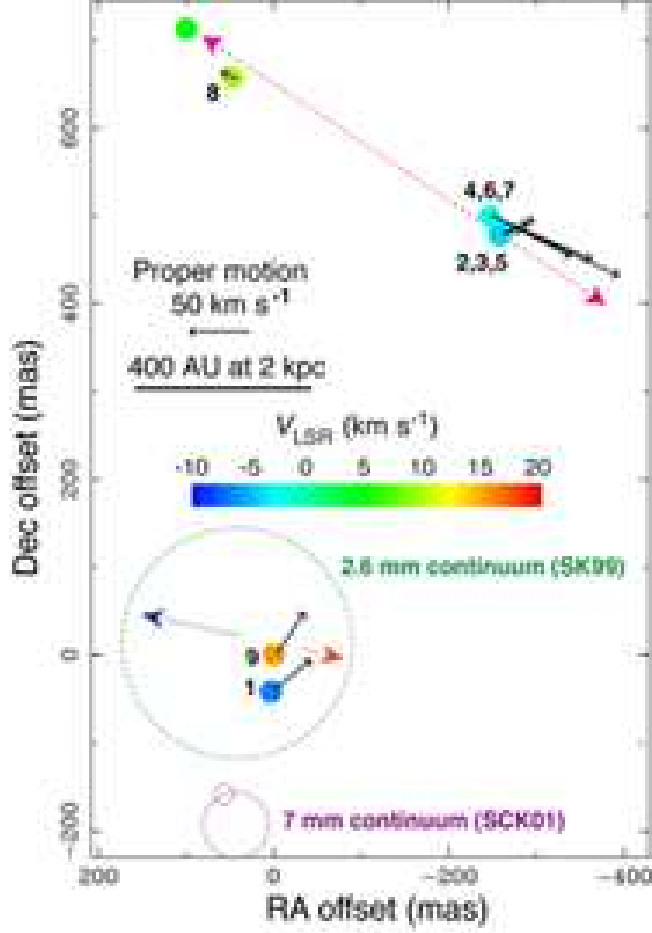


**Fig. 2.** Doppler velocity distribution (colored filled circle) and relative proper motions (black arrow) of  $\text{H}_2\text{O}$  masers in G192.16–3.84. The displayed proper motion vector is that subtracted by a velocity bias  $(\overline{\Delta V}_x, \overline{\Delta V}_y) = (23, -34) [\text{km s}^{-1}]$  from the original vector so that the northern jet source is spatially fixed. A number added for each feature with a proper motion shows the assigned one after the designated name form “G192.16–3.84: I2006”. The map origin is located at R.A.(J2000.0)= $05^{\text{h}}58^{\text{m}}13^{\text{s}}.5332$ , decl.(J2000.0)= $+16^{\circ}31'58''.483$ , which was estimated as described in the main text. The locations of 2.6 mm and 7 mm continuum emission peaks estimated by SK99 and SCK01, respectively, are roughly indicated by dashed circles. Axes of the northern jet and the outer outflow proposed by SBCSK04 are indicated by dashed arrow.

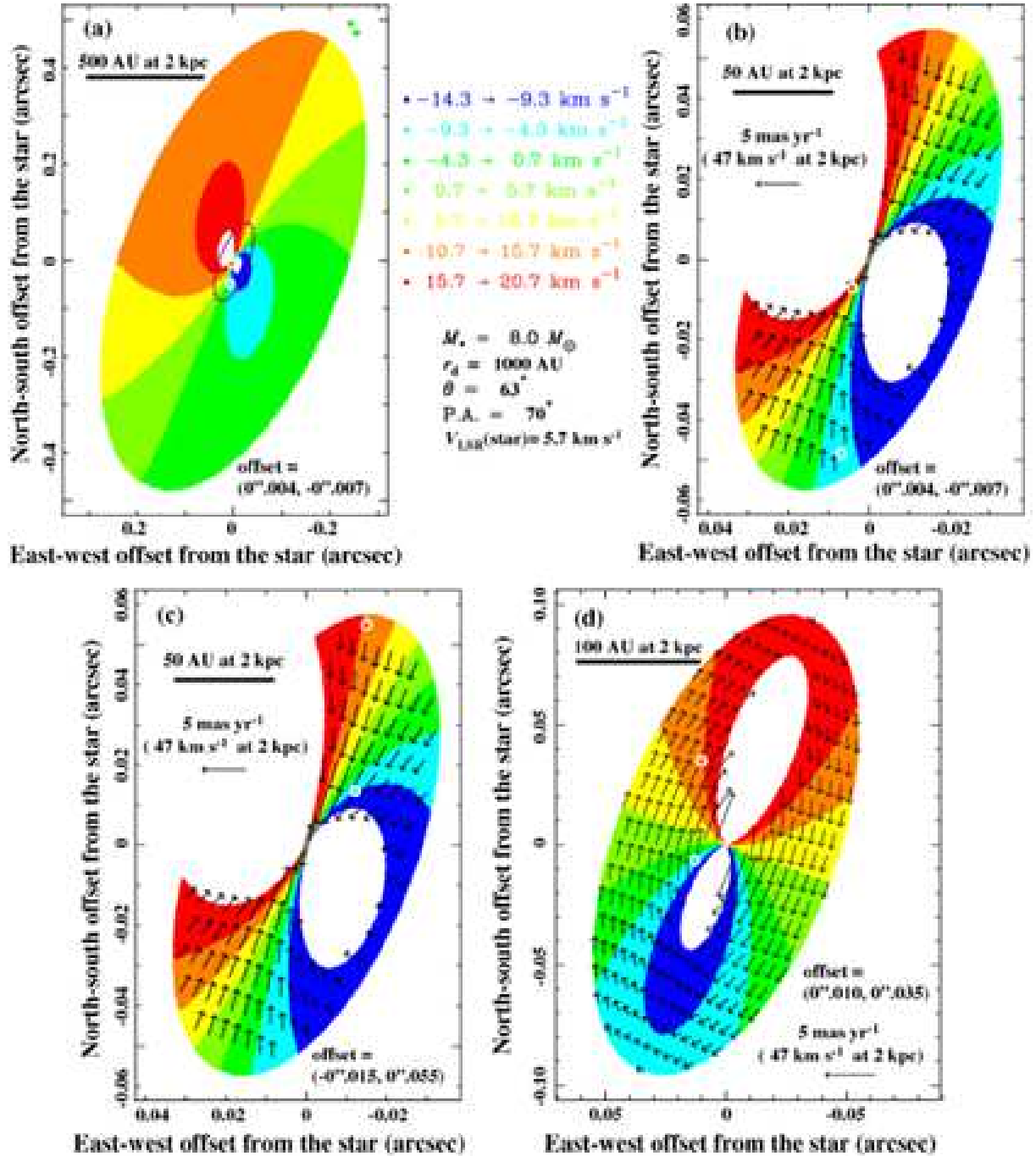


**Fig. 3.** Calculated LSR-velocity distribution for masing gas clumps on the modeled thin disks. The  $\text{H}_2\text{O}$  maser features displayed in figure 2 (filled circles) are overlaid after shifting the offset coordinates by the value shown in the sub-panels. All of the models adopt the same physical parameters of the disk, except for the velocity field. (a) A disk model with impinging maser clumps, which is best consistent with the observed maser kinematics. The two maser features are located at the southern part on the disk. The whole disk with an apparent radius of  $\leq 0''.5$  is displayed. A dashed purple ellipse indicates a displayed region of the same disk in (b). (b) Same as (a) but displaying the inner part of the disk. An arrow indicates a proper motion of the gas clump located at the root of the arrow. (c) Same as (b) but the maser features are located at the northern part on the disk. (d) A purely Keplerian-rotating disk model.

**Table 1.** Status of the telescopes, data reduction, and resulting performances in the individual epochs of the JVN observations.

Observation code	Epoch in the year 2005	Duration (hr)	Used telescopes <sup>1</sup>	Reference velocity <sup>2</sup> (km s <sup>-1</sup> )	1- $\sigma$ level noise (mJy beam <sup>-1</sup> )	Synthesized beam <sup>3</sup> (mas)	Number of detected features
r05084a ...	March 25	10	MZ, IR, OG, IS, KS, NB <sup>4</sup>	15.8	40	4.6×0.9, -35°	10
r05117a ...	April 27	10	MZ, IR, OG, IS <sup>5</sup> , KS, NB	15.6	26	1.7×1.0, -44°	13
r05152a ...	June 1	8	MZ, OG <sup>5</sup> , IS <sup>5</sup> , KS, NB	-0.8	60	1.6×0.9, -48°	7

<sup>1</sup> Telescopes that were effectively operated and whose recorded data were valid: MZ: the VERA 20 m telescope at Mizusawa, IR: the VERA 20 m telescope at Iriki, OG: the VERA 20 m telescope at Ogasawara Is., IS: the VERA 20 m telescope at Ishigakijima Is., KS: the NiCT 34-m telescope at Kashima, NB: the NRO 45-m telescope at Nobeyama.

<sup>2</sup> Velocity channel used for the phase reference in data reduction.

<sup>3</sup> The synthesized beam made in natural weight; major and minor axis lengths and position angle.

<sup>4</sup> Ceasing operation for 7 hrs due to strong winds.

<sup>5</sup> High system temperature (>300 K) due to bad weather conditions.

**Table 2.** Parameters of the H<sub>2</sub>O maser features identified by proper motion toward G192.16–3.84.

Maser feature <sup>1</sup> (G192.16–3.84: I2006)	Offset <sup>2</sup> (mas)		Proper motion <sup>2</sup> (mas yr <sup>-1</sup> )				Radial motion <sup>3</sup> (km s <sup>-1</sup> )		Peak intensity at three epochs (Jy beam <sup>-1</sup> )		
	R.A.	decl.	$\mu_x$	$\sigma\mu_x$	$\mu_y$	$\sigma\mu_y$	$V_z$	$\Delta V_z$ <sup>4</sup>	Epoch 1	Epoch 2	Epoch 3
1 <sup>5</sup> .....	2.90	-41.46	-0.78	0.39	-1.03	0.20	-6.76	1.05	1.93	2.44	5.87
2 .....	-258.37	479.06	-0.34	0.58	-2.26	0.24	-3.59	0.49	1.63	1.70	0.99
3 .....	-259.06	479.24	0.23	2.38	-2.64	0.67	-2.96	0.52	1.32	0.83	...
4 .....	-246.15	500.19	-4.56	0.52	-7.15	0.38	-2.76	0.84	2.18	... <sup>6</sup>	0.61
5 .....	-260.82	479.38	0.93	0.86	-3.12	0.13	-2.65	0.84	3.80	3.75	1.99
6 .....	-246.24	500.08	-6.39	0.26	-7.45	0.21	-1.73	2.32	5.10	5.85	47.60
7 .....	-246.61	499.88	-8.80	1.20	-8.87	0.95	-0.85	0.47	0.38	1.18	...
8 .....	46.63	657.13	3.74	0.79	-2.99	0.79	9.86	0.47	...	0.88	0.69
9 <sup>7</sup> .....	0.00	0.00	0.00	0.13	0.00	0.47	15.87	1.76	9.19	12.29	7.59

<sup>1</sup> Water-maser features detected toward G192.16–3.84. The feature is designated as G192.16–3.84:I2006 *N*, where *N* is the ordinal source number given in this column (I2006 stands for sources found by Imai et al. and listed in 2006).

<sup>2</sup> Relative value with respect to the motion of the position-reference maser feature: G192.16–3.84:I2006 *9*.

<sup>3</sup> Relative value with respect to the local stand of rest.

<sup>4</sup> Mean full velocity width of a maser feature at half intensity.

<sup>5</sup> The maser feature A (see main text).

<sup>6</sup> The maser feature was spatially overlapped with the maser feature G192.16–3.84:I2006 *6* and its peak intensity was unable to evaluated.

<sup>7</sup> The maser feature B (see main text).

**Table 3.** Diagonalization analysis of the variance-covariance matrix of the velocity and position vectors of the G192.16–3.84 H<sub>2</sub>O masers.

Eigenvector		
Eigenvalue [(km <sup>-1</sup> ) <sup>2</sup> ]	Inclination	Position angle
Velocity variance-covariance matrix		
2502 ± 306	2°.0 ± 0°.5	59°.6 ± 2°.9
106 ± 49	–20°.0 ± 7°.8	–29.3 ± 8°.7
Spatial variance-covariance matrix (mas <sup>2</sup> )		
16939	...	60°.6